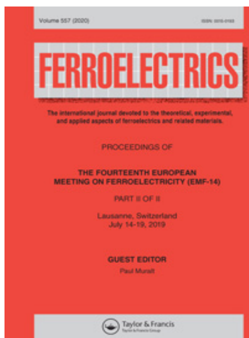

Ferroelectrics

ISSN: 0015-0193 (Print) 1563-5112 (Online) Journal homepage: https://www.tandfonline.com/loi/gfer20

Comparison of amplification via the acousto-electric effect of Rayleigh and Leaky-SAW modes in a monolithic surface InP:InGaAs/lithium niobate heterostructure

Aleem M. Siddiqui, Lisa P. Hackett, Daniel Dominguez, Anna Tauke-Pedretti, Tom Friedmann, Gregory Peake, Michael R. Miller, James K. Douglas & Matt Eichenfield

To cite this article: Aleem M. Siddiqui, Lisa P. Hackett, Daniel Dominguez, Anna Tauke-Pedretti, Tom Friedmann, Gregory Peake, Michael R. Miller, James K. Douglas & Matt Eichenfield (2020) Comparison of amplification via the acousto-electric effect of Rayleigh and Leaky-SAW modes in a monolithic surface InP:InGaAs/lithium niobate heterostructure, Ferroelectrics, 557:1, 58-65

To link to this article: https://doi.org/10.1080/00150193.2020.1713363

© 2020 The Authors. Published with license by Taylor & Francis Group, LLC.

Published online: 07 Apr 2020.

Submit your article to this journal

Article views: 171

View related articles

View Crossmark data

Full Terms & Conditions of access and use can be found at
https://www.tandfonline.com/action/journalInformation?journalCode=gfer20

FERROELECTRICS
2020, VOL. 557, 58–65
https://doi.org/10.1080/00150193.2020.1713363

Taylor & Francis
Taylor & Francis Group

OPEN ACCESS Check for updates

Comparison of amplification via the acousto-electric effect of Rayleigh and Leaky-SAW modes in a monolithic surface InP:InGaAs/lithium niobate heterostructure

Aleem M. Siddiqui, Lisa P. Hackett, Daniel Dominguez, Anna Tauke-Pedretti, Tom Friedmann, Gregory Peake, Michael R. Miller, James K. Douglas, and Matt Eichenfield

Sandia National Laboratory, Albuquerque, New Mexico, USA

ABSTRACT
This paper demonstrates a monolithic surface acoustic wave amplifier fabricated by state-of-the-art heterogenous integration of a III-V InGaAs-based epitaxial material stack and $LiNbO_3$. We compare amplification of Raleigh-SAW and leaky-SAW modes on a on Y-cut, X-propagating delay line amplifier. Due to the superior properties of the materials employed, we observe a net terminal gain of 3dB for an LSAW overtone mode This platform enables further advances in active and non-reciprocal piezoelectric acoustic devices.

ARTICLE HISTORY
Received 14 July 2019
Accepted 24 December 2019

KEYWORDS
Acousto-electric effect; heterogeneous integration; surface acoustic waves

1. Introduction

Active and non-reciprocal piezoelectric acoustics employing the acoustoelectric (AE) effect have the potential to transform RF signal processing by miniaturizing devices such as amplifiers, isolators, and oscillators. This effect exhibited tremendous potential early on, with many demonstrations from 1960's to the early 1980's of devices ranging from amplifiers with 10's of dB of gain per centimeter to delay lines with 100 dB of non-reciprocity [1–4]. However, high power consumption and large operating voltages prevented widespread adoption of the technology. Practical AE devices require that the semiconductor be thin, have low doping, high mobility, and low density of trap states. Simultaneously, the piezoelectric layer requires a propagating mode with low loss and large electro-mechanical coupling coefficient, K^2. More recently, continued development of piezo-electric and semiconductor materials has led to promising results for practical implementation of AE devices. A large AE effect was shown in $GaAs/LiNbO_3$ (LNO) with high mobility and low doping [5]. Additionally, graphene and other material platforms, such as LNO and GaN, have been explored as part of renewed interest in simultaneous transmit and receive applications (STAR) [6–8].

In this work, we leverage recent advances in the fields of epitaxial semiconductor materials, heterogeneous integration, and piezoelectric ultra-thin-film processing to

CONTACT Aleem M. Siddiqui asiddiq@sandia.gov
Color versions of one or more of the figures in the article can be found online at www.tandfonline.com/gfer.

© 2020 The Authors. Published with license by Taylor & Francis Group, LLC.
This is an Open Access article distributed under the terms of the Creative Commons Attribution-NonCommercial-NoDerivatives License (http://creativecommons.org/licenses/by-nc-nd/4.0/), which permits non-commercial re-use, distribution, and reproduction in any medium, provided the original work is properly cited, and is not altered, transformed, or built upon in any way.

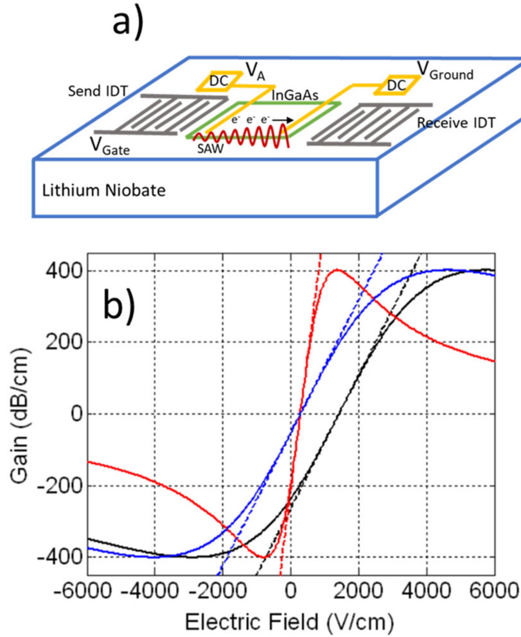

Figure 1. (a) Schematic of the InGaAs-$LiNbO_3$ heterostructure SAW amplifier. (b) Gain profile scaling with increasing mobility (black curve to blue curve) and decreasing density (blue curve to red curve).

overcome the noise performance and efficiency obstacles faced by the older technology. Reduction of the semiconductor defect-induced diffusivity must be accomplished in a way that still allows it to achieve an intimate contact with the LNO. Previously we have developed heterogeneous integration techniques for the transfer of epitaxial III-V semiconductor films using silicon nitride as a bonding interface [9, 10]. We have also demonstrated the ability to grow high-quality silicon nitride films on our thin $LiNbO_3$ membranes. Combining these, we believe we can achieve thermal-diffusion-limited InP:InGaAs films with 25x the mobility of the films used in [1–4]. While SAW amplifiers may have been impractical in the past due to limitations on material properties, here we have leveraged Sandia's Microfabrication capabilities to yield practical, functional devices in a heterogeneously integrated platform, through higher mobility and lower defect-induced trap states essentially leading to low voltage, low noise, high gain amplifiers.

2. AE gain expression

In the AE effect, SAW waves in a piezo-electric layer are amplified or attenuated due to the screening interaction between drifting carriers in an adjacent semiconductor and the SAW evanescent electric field through an interaction similar to traveling wave tube amplifier [11] as shown in Figure 1a. The gain experienced by a SAW wave due to the AE effect (i.e. electronic gain) is determined as $P_{out} = P_{in}e^{\Gamma \times L}$, where Γ is set by following expression, which is plotted in Figure 1b:

$$\Gamma = K^2 \frac{\pi}{\lambda} \times \frac{x}{1 + (x)^2}, \quad x = \left(\frac{\mu E}{v_A} - 1\right)\frac{\sigma_m}{\sigma} \tag{1}$$

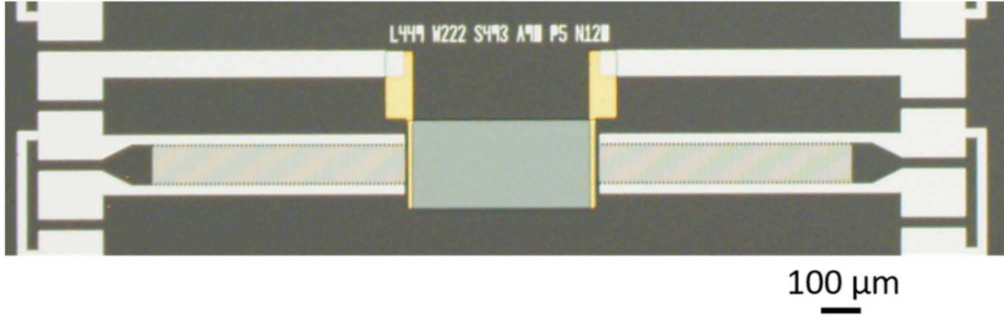

Figure 2. Microscope image of the fabricated Rayleigh wave amplifiers.

Here, K^2 is the electromechanical coupling, λ is the acoustical wavelength, v_A is the speed of sound, $\sigma = en\mu \times d$ is the sheet conductance, $\sigma_m = (\varepsilon_P + \varepsilon_0)v_A$ is a material dependent parameter, μ is the mobility and E is the local electric field supplied as a voltage applied across the semiconductor slab. An electronic gain of 0dB (i.e. unity gain) is achieved when the speed of the drifting carriers matches the acoustical velocity. For a device with a given length L, this voltage can be expressed as:

$$V_{0dB} = E_{0dB} \times \mathrm{L} = \frac{v_A}{\mu} \times L \tag{2}$$

To achieve gain, additional voltage beyond V_{0dB} needs to be applied. Our goal here is to relate the voltage needed to achieve a targeted gain via Equation (1) by linearizing Equation (1) about the 0dB point (see Figure 2.) Thus, to achieve a target gain, dB_T, the total applied voltage must account for both V_{0dB} and the access field: $V_{Tot} = V_{0dB} + \Delta V_{dB}$. Linearized about the 0dB point the excess field can be expressed via the slope, m, of the gain curve:

$$\Delta \boldsymbol{V}_{dB} = \frac{\boldsymbol{dB_T}}{\boldsymbol{m}}, \quad \boldsymbol{m} = \ 0.0869 \times \boldsymbol{K}_r^2 \frac{\boldsymbol{\pi}}{\boldsymbol{\lambda}} \left(\frac{\boldsymbol{\varepsilon_P} + \varepsilon_0}{\boldsymbol{d} \times \boldsymbol{e} \times \boldsymbol{n}} \right) \tag{3}$$

Figure 1(b) shows the gain profile scaling with increasing mobility (black curve to blue curve) and decreasing density (blue curve to red curve). Large gain at low voltages, therefor requires low density and high mobility.

2.1. Epitaxial and piezoelectric device fabrication

The SAW amplifier presented here requires heterogenous integration of a III-V epitaxial semiconductor material stack with a $LiNbO_3$ piezoelectric acoustic device. Toward this objective, a fabrication flow was developed where wafer bonding between the epitaxial layers and the $LiNbO_3$ wafer was carried out, and complete amplifiers were fabricated.

2.1.1. Process flow

The fabrication process flow is shown in Figure 3. The epitaxial stack, grown by metal-organic chemical vapor deposition (MOCVD), consists of a 2 nm InP capping layer (not shown in Figure 3), a 100 nm InGaAs amplifier layer, a 100 nm InP etch stop layer, and a 100 nm InP contact layer on a 2-inch InP wafer. The InP wafer with the epitaxial

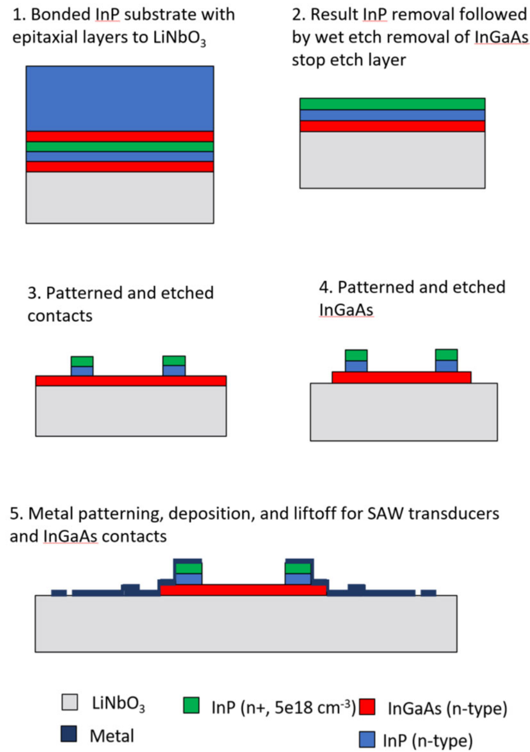

Figure 3. Process flow for Rayleigh wave amplifiers utilizing a III-V epitaxial semiconductor stack bonded to a y-cut $LiNbO_3$ wafer.

stack is first bonded to a y-cut $LiNbO_3$ wafer. The bulk of the InP substrate is then removed leaving approximately 50 μm. The wafer is then etched in HCl to remove the remaining InP followed by removal of the InGaAs etch stop layer in a piranha solution.

A highly doped InP (n-type, 5e18 cm-3) layer is utilized to assist in making electrical contact to the InGaAs amplifier layer. The InP contact layer is patterned by photolithography and wet-etched. This is followed by patterning and wet etching of the InGaAs amplifier layer. To finalize the fabrication of these devices, two metal lift-of processes are carried out. The first utilizes a metal stack consisting of silver (Ag) and gold (Au) with a titanium (Ti) adhesion layer to make contact to the InGaAs amplifier through the InP contact layer. The second consists of aluminum (Al) with chrome (Cr) adhesion layer to fabricate the SAW transducers.

2.1.2. Fabricated SAW amplifiers

A high-quality bond between the InP substrate with the epitaxial semiconductor layers and the $LiNbO_3$ wafer is crucial for fabrication of these devices. We have demonstrated successful wafer bonding, which is attributed to the quality and flatness of the epitaxial stack, as shown by the atomic force microscope (AFM) scans in Figure 4 where only sub-nm growth steps are observed. A successfully bonded wafer is shown in the lower panel of Figure 4 where bubbles appear only in at the periphery of the epitaxial stack, which we attribute to minimal polycrystalline protrusions.

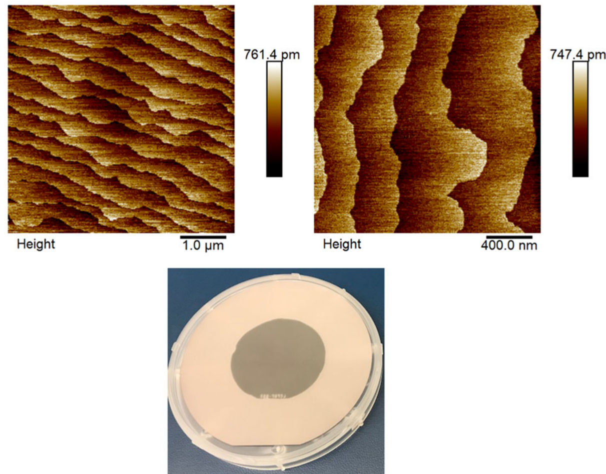

Figure 4. Upper two panels: AFM scans of the epitaxial stack before bonding to the LiNbO3 wafer. Lower panel: bonded stack on the LiNbO3 wafer. Successful bonding is attributed to the quality and flatness of the layers.

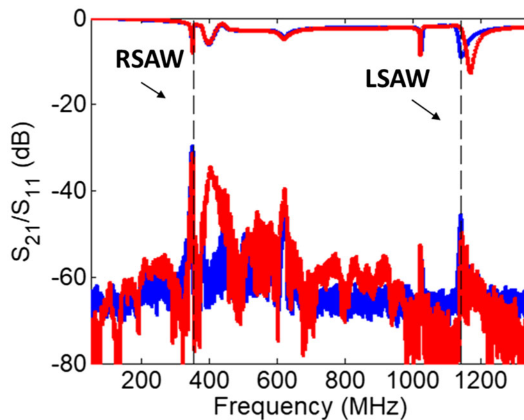

Figure 5. S-parameter measurements for a delay device with Length = 1 mm, Width = 429 µm, Transducer: $N_{fingers} = 90$, pitch = 50 µm, Aperture = 210 µm. Red indicates $S_{21}/S1_1$ and blue indicates S_{12}/S_{22}.

A microscope image of the completed SAW amplifiers is shown in Figure 2. The devices consist of two SAW transducers with a rectangular InGaAs layer in the center. Electrical contact is made to the InGaAs by contact pads that terminate as strips along each end of the patterned semiconductor. It is clear that our fabricated amplifiers can be made with few defects over the given semiconductor surface area.

3. Experimental results

SAW devices comprised of straight fingered interdigitated electrodes in a send/receive configuration with amplifier region positioned in the delay region. Figure 5 show the S-parameters for a device with the following parameters: finger number = 60,

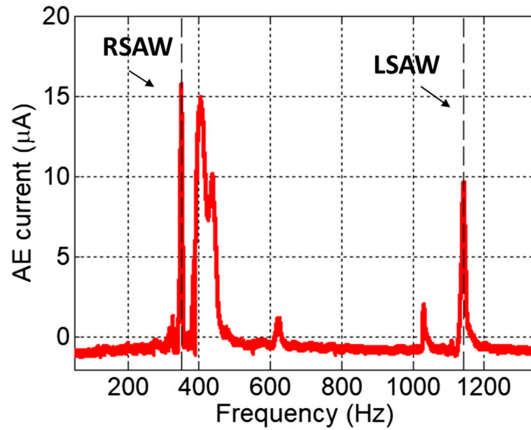

Figure 6. DC current due to the AE interaction measured while the frequency is swept during S-parameter measurements taken in Figure 5.

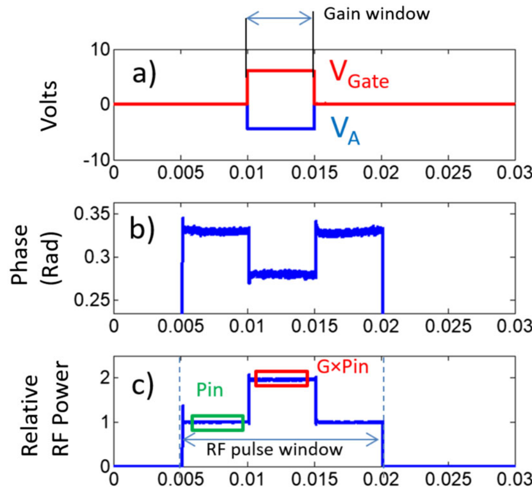

Figure 7. The experimental procedure including the applied voltage pulses, measured phase shift, and measured increase in RF power is shown.

pitch = 10.5 μm, aperture = 210 μm. Additionally fingers are oriented on a Y-cut black lithium niobite wafer oriented so that the launched wave is X-propagating. As indicated in the Figures 5 and 6, the send/receive ports couple to both Rayleigh SAW (RSAW), which are known to have a coupling coefficient of a 5%, and Leaky SAW (LSAW) modes which have a larger coupling coefficient of nearly 15% with attenuation [11]. To confirm AE interaction, the generated DC current due to RF power being dissipated in space charge is measured while the frequency is swept. The measured current vs frequency mirrors the S_{21} data confirming coupling between SAW/LSAW modes and carriers in the InGaAs layer.

To evaluate gain, the transmission of a pulsed RF signal from the send to receive transducers and is measured with a spectrum analyzer during the application of a voltage pulse across the semiconductor (VA). Figure 7 shows the applied voltage pulses, phase shift, and pulsed RF signal increase during a measurement sequence, indicating a

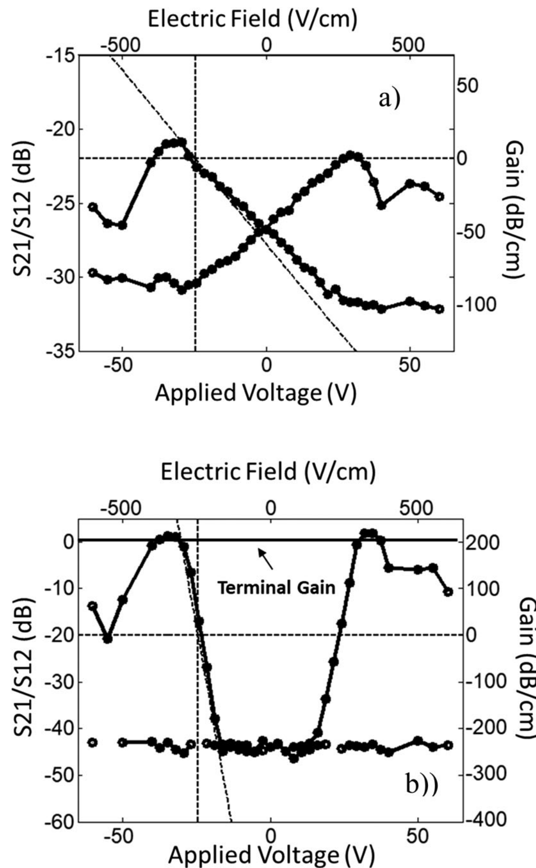

Figure 8. Increase in S_{21}/S_{12} due to the AE amplification during the application of a voltage pulse while the NA frequency was fixed. (a) Shows the gain at 330MHz corresponding to the RSAW modes indicated in Figures 5 and 6 while (b) shows the gain at 1.2GHz corresponding to the LSAW mode.

high degree of measurement fidelity. Figure 8 show the increase/decrease of S_{21}/S_{12} during the application of a voltage pulse for the fundamental RSAW and an overtone LSAW. The RSAW and LSAW frequencies are indicated in Figures 5 and 6. We observe that the that the slope of the gain near the 0dB point increase by nearly a factor of 5 for the LSAW compared to the RSAW mode confirming the expected increase in coupling coefficient. The resulting large gain enables us to achieve a terminal gain of 3dB at 1.2GHz in the LSAW overtone mode.

4. Conclusion

In conclusion, we have developed a monolithic SAW amplifier with state-of-the-art heterogeneous integration of III-V epitaxial material stack (InGaAs) and $LiNbO_3$. We have demonstrated that improvements in semiconductor material parameters have enabled performance metrics beyond the limitations historically faced by similar past device designs. The results presented in this work are a first step toward developing practical, high performance SAW amplifiers based on the acoustoelectric effect.

Funding

Sandia National Laboratories is a multi-mission laboratory managed and operated by NTESS of Sandia, LLC., a wholly owned subsidiary of Honeywell International, Inc., for the U.S. Department of Energy's National Nuclear Security Administration under contract DE-NA0003525. This work was supported by the Laboratory Directed Research and Development Program. The views, opinions, and/or findings expressed are those of the author(s) and should not be interpreted as representing the official views or policies of the Department of Defense or the U.S. Government.

References

[1] L. A. Coldren and G. S. Kino, Monolithic acoustic surface-wave amplifier, *Appl. Phys. Lett*. **18** (8), 317 (1971). DOI: 10.1063/1.1653677.

[2] R. M. White, Surface elastic-wave propagation and amplification, *IEEE Trans. Electron Devices* **14** (4), 181 (1967). DOI: 10.1109/T-ED.1967.15926.

[3] K. Yoshida and M. Yamanishi, Interaction between surface elastic waves and drifting carriers in layered system, *Jpn. J. Appl. Phys*. **7** (9), 1143 (1968). DOI: 10.1143/JJAP.7.1143.

[4] G. S. Kino and L. A. Coldren, Noise figure calculation for the Rayleigh wave amplifier, *Appl. Phys. Lett*. **22** (1), 50 (1973). DOI: 10.1063/1.1654471.

[5] M. Rotter *et al.*, Giant acoustoelectric effect in GaAs/LiNbO3 hybrids, *Appl. Phys. Lett*. **73** (15), 2128 (1998). DOI: 10.1063/1.122400.

[6] S. Ghosh, M. A. Hollis, and R. J. Molnar, Acoustoelectric amplification of Rayleigh waves in low sheet density AlGaN/GaN heterostructures on sapphire, *Appl. Phys. Lett*. **114** (6), 063502 (2019). DOI: 10.1063/1.5080450.

[7] C. P. Carmichael *et al.*, Experimental investigation of surface acoustic wave acoustoelectric effect using a graphene film on lithium niobate, *IEEE Trans. Ultrason., Ferroelect., Freq. Contr*. **65** (11), 2205 (2018). DOI: 10.1109/TUFFC.2018.2870042.

[8] U. K. Bhaskar, S. A. Bhave, and D. Weinstein, Silicon acoustoelectronics with thin film lithium niobate, *J. Phys. D: Appl. Phys*. **52** (5), 05LT01 (2019). DOI: 10.1088/1361-6463/aaee59.

[9] A. Tauke-Pedretti *et al.*, Integrating III-V compound semiconductors with silicon for advanced multijunction solar cells, Sandia National Lab. (SNL-NM), Albuquerque, NM (United States), SAND2015-0772C, Feb. 2015.

[10] A. Tauke-Pedretti *et al.*, Bonded InGaAs cells for microsystems enabled photovoltaics, *2014 IEEE 40th Photovoltaic Specialist Conference (PVSC)*, Denver, CO, 2014, p. 0546–0549.

[11] B. A. Auld and G. S. Kino, Normal mode theory for acoustic waves and its application to the interdigital transducer, *IEEE Trans. Electron Devices* **18** (10), 898 (1971). DOI: 10.1109/T-ED.1971.17303.